IUST
Iran University of Science and Technology

Iranian Journal of Electrical and Electronic Engineering

Journal Homepage: ijeee.iust.ac.ir

Research Paper

Robust H_∞-Primary Control of AC Islanded Microgrids based on LPV Modeling

F. Zare-Mirakabad*, M. H. Kazemi*(C.A.) and A. Doroudi*

Abstract: This paper proposes a robust H_∞-LMI-based primary controller using the Linear Parameter Varying (LPV) modeling for an AC Islanded Microgrid (IMG). The proposed controller can regulate the frequency and voltage of the IMG under various scenarios, such as load changes, faults, and reconfigurations. Unlike most previous studies that neglected the nonlinearity and uncertainty of the system, this paper represents the system dynamics as a polytopic LPV model in the novel primary control structure. The proposed method computes a state-feedback control by solving the corresponding Linear Matrix Inequalities (LMIs) based on H_∞ performance and stability criteria. The robust primary control is applied to a test IMG in the SIM-POWER environment of MATLAB and evaluated under different scenarios. The simulation results demonstrate the effectiveness and efficiency of the proposed method in maintaining the stability of the frequency and voltage of the IMG.

Keywords: Robust Control, AC Islanded Microgrid, Primary Control, Nonlinearity, Uncertain Parameter.

1 Introduction

THE microgrid (MG) is becoming increasingly popular for various reasons, including economic considerations, technological advances, concerns about environmental problems, climate change, and rising levels of consumer demand. MG decreases greenhouse gas emissions, improves power quality and flexibility, has the local capability to solve energy problems, and reduces energy losses and transmission-line loading. In addition to all of these benefits, it is utilized as an effective method for integrating renewable energy systems.

The MG is a small-scale active power distribution grid that operates at the low-voltage level and incorporates distributed energy resources, local loads, power electronics, and protection systems. It acts as a controllable unit under the monitoring of the control system, conforming to the Central Grid [1-5].

Iranian Journal of Electrical & Electronic Engineering, 2023. First received 30 Nov 2022 and accepted 13 Sep 2023.
* The authors are with the Department of Electrical Engineering, Shahed University, Tehran, Iran.
E-mails: fatemeh.zare@shahed.ac.ir, kazemi@shahed.ac.ir, and doroudi@shahed.ac.ir.
Corresponding Author: MH. Kazemi.
https://doi.org/10.22068/IJEEE.19.3.2724

The MG is a small-scale active power distribution grid that operates at the low-voltage level and incorporates distributed energy resources, local loads, power electronics, and protection systems. It acts as a controllable unit under the monitoring of the control system, conforming to the Central Grid [1-5].

The MG can operate in two distinct modes, namely, the connected mode and the island mode. The regulation of voltage and frequency in the AC grid-connected mode depends on the operation of the reference grid. As a result of this phenomenon, the controllers are utilized to regulate both active and reactive powers to enhance the quality of management. In the AC islanded mode, the MG operates autonomously independently from the utility grid. Consequently, the controllers modify the frequency and voltage by properly sharing active and reactive power [6-8].

The hierarchical control approach is a frequently encountered control structure for MGs in grid-connected and island modes. This methodology employs a tripartite system of control comprising primary, secondary, and tertiary levels. The primary control system maintains voltage and frequency at stable levels and ensures proper power sharing. The secondary control mechanism mitigates the frequency and voltage fluctuations from the primary level while ensuring synchronization between the MG and the central grid.

The optimized performance of the MG in both connected and islanded modes is attributed to the implementation of tertiary control, which facilitates power flow regulation between the central grid and the MG [7, 9]. The work [10] presents an H_∞ consensus-based control system for AC heterogeneous autonomous MGs, ensuring stability and robustness using Lyapunov-Krasovskii theory. The system regulates voltage and frequency, providing accurate power-sharing and state-of-charge modification. A novel H_∞ theory-based resilient distributed cooperative control strategy for off-grid AC MG's secondary control layer addresses disturbances, uncertainty, and stability conditions proposed in [11]. Nonlinearities and uncertainties are inherent in real-world engineering systems, posing challenges for theoretical analyses and control system design. Typically, physical components within control systems, such as controllers and actuators, experience saturation. Conversely, physical methods are replete with uncertainties, necessitating the incorporation of such uncertainties into the control system's design. A pertinent practical concern that warrants consideration in multiagent systems pertains to the unreliability of communication networks. [12]. When linear time-invariant approaches fail, nonlinearity modeling in LPV structures can synthesize controllers [13, 14]. The neural network-based adaptive LPV controller for DC MG power system is proposed in [15]. The work [16] describes grid-following inverter control methods. LPV-power-synchronized control works in strong and weak grids. Model-based predictive control uses a hybrid H_2/H_∞ linear time-varying state feedback architecture described in [17]. An MG's inverter LPV model considered disturbances and uncertainties. The work [18] examines polytopic quasi-LPV and sliding mode fault detection and reconstruction in DC MGs with nonlinear loads. The work [19] examines frequency fluctuation dampening with a strong LPV control in an islanded hybrid MG system. LPV hides the nonlinearity of the wind turbine's wind and rotation speeds, which are scheduling parameters.

This paper provides a robust H_∞-LMI-based primary controller for an AC IMG that considers load bar change, faults, and reconfiguration situations to control the stability of frequency and voltage of MG. Unlike most previous efforts, which neglected the model's nonlinearity and uncertainty, the system's nonlinearity and uncertain parameters are considered as a Polytopic LPV framework in this paper's innovative proposed primary control structure. A state-feedback control is generated in the provided approach by solving the required LMIs described on the executed polytopic LPV model based on H_∞ performance and stability to assess the control signals. Under load bar change, fault, and reconfiguration scenarios, the proposed robust primary control applies to the Test-IMG in the SIM-POWER environment of MATLAB. The simulation results indicate the suggested technique's effectiveness and efficiency in handling the MG's frequency and voltage and correct power-sharing.

2 Preliminaries

2.1 Proposed Primary Control Preliminaries

This section presents the preliminary primary control proposals. The principal mechanism attains a plug-and-play operational capability for the MG while preserving frequency and voltage constancy. Figure 1 depicts the functional block diagram of the voltage source inverter (VSI) distributed generation (DG) module, incorporating a proposed robust primary control. The MG comprises multiple DG modules that synchronize to maintain a stable voltage and frequency range. The symbol δ_i denotes the angular orientation of the DG_i reference frame relative to a shared reference frame and satisfies the following equation.

$$\dot{\delta}_i = \omega_i - \omega_s \tag{1}$$

where ω_i is the angular frequency of rotation of the DG_i, and ω_s represents the same dependent with the standard reference frame.

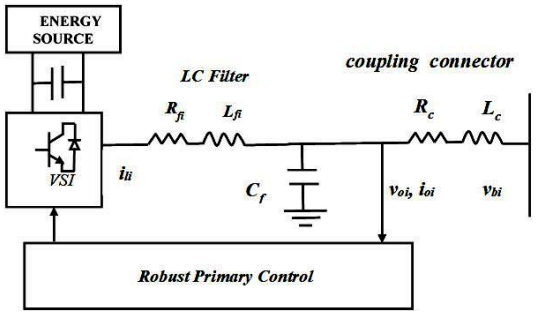

Fig. 1 The operating block diagram of the VSI-based DG module with the proposed robust primary control.

The following equations rule the frequency and voltage droop factors wielded by the primary controller.

$$\omega_i = \omega^* - m_{Pi} P_i \tag{2}$$

$$v^*_{odi} = v_{in} - n_{Qi} Q_i \tag{3}$$

$$v^*_{oqi} = 0 \tag{4}$$

where m_{Pi} and n_{Qi} are the droop factor. The P_i and Q_i symbolize the active power and reactive power measured at the terminals of the DG_i, respectively. The reference frequency and voltage of the droop controller are ω^* and v_{in}. The equations of the power loop in the robust primary controller, shown in Fig. 2, can be written as:

$$\dot{P}_1 = -\omega_{ci} P_i + \omega_{ci} (v_{odi} i_{odi} + v_{oqi} i_{oqi}) \tag{5}$$

$$\dot{Q}_i = -\omega_{ci} Q_i + \omega_{ci} (-v_{odi} i_{oqi} + v_{oqi} i_{odi}) \tag{6}$$

$$\dot{\phi}_{di} = v^*_{odi} - v_{odi} \tag{7}$$

$$\dot{\phi}_{qi} = v^*_{oqi} - v_{oqi} \tag{8}$$

The direct and quadrature (dq) components of v_{oi} and i_{oi}, as exhibited in Fig. 1, are v_{odi}, v_{oqi}, i_{odi} and i_{oqi}, respectively. The ω_{ci} is the cut-off frequency of the low-pass filter (LPF). The ϕ_{di} and ϕ_{qi} are part of the defined state variables [20-22].

The equations of the voltage loop in the robust primary controller, shown in Fig. 3, are expressed as:

$$i^*_{ldi} = F_i i_{odi} - \omega_b C_{fi} v_{oqi} + k_p v_{in} + u_1 \tag{9}$$

$$i^*_{lqi} = F_i i_{oqi} + \omega_b C_{fi} v_{odi} + u_3 \tag{10}$$

$$\dot{\gamma}_{di} = i^*_{ldi} - i_{ldi} \tag{11}$$

$$\dot{\gamma}_{qi} = i^*_{lqi} - i_{lqi} \tag{12}$$

where ω_b is the nominal angular frequency and F_i is local gain, and the state variables are γ_{di} and γ_{qi}. C_{fi} is the capacitance of the LPF. u_1 and u_3 are control inputs. The equations of the current loop in the robust primary controller, shown in Fig. 4, can be expressed as:

$$v^*_{idi} = -\omega_b L_{fi} i_{lqi} + u_2 \tag{13}$$

$$v^*_{iqi} = \omega_b L_{fi} i_{ldi} + u_4 \tag{14}$$

where L_{fi} is the inductance of the LPF. u_2 and u_4 are control inputs. i_{ldi} and i_{lqi} are the dq components of i_{li} as exhibited in Fig. 1.

The equation of the output LC filter and coupling connector, as exhibited in Fig. 1, can be expressed as:

$$\dot{i}_{ldi} = -\frac{R_{fi}}{L_{fi}} i_{ldi} - \frac{1}{L_{fi}} v_{odi} + \frac{1}{L_{fi}} u_2 \tag{15}$$

$$\dot{i}_{lqi} = -\frac{R_{fi}}{L_{fi}} i_{lqi} - \frac{1}{L_{fi}} v_{oqi} + \frac{1}{L_{fi}} u_4 \tag{16}$$

$$\dot{v}_{odi} = \frac{1}{C_{fi}} i_{ldi} - \frac{1}{C_{fi}} i_{odi} + \omega^* v_{oqi} - m_{Pi} P_i v_{oqi} \tag{17}$$

$$\dot{v}_{oqi} = -\omega^* v_{odi} + m_{Pi} P_i v_{odi} + \frac{1}{C_{fi}} i_{lqi} - \frac{1}{C_{fi}} i_{oqi} \tag{18}$$

$$\dot{i}_{odi} = -\frac{R_{ci}}{L_{ci}} i_{odi} + \omega^* i_{oqi} - m_{Pi} P_i i_{oqi} + \frac{1}{L_{ci}} v_{odi} + d_1 \tag{19}$$

$$\dot{i}_{oqi} = \frac{-R_{ci}}{L_{ci}} i_{oqi} - \omega^* i_{odi} + m_{Pi} P_i i_{odi} + \frac{1}{L_{ci}} v_{oqi} + d_2 \tag{20}$$

where $d_1 = \frac{1}{L_{ci}} v_{bdi}$, $d_2 = \frac{1}{L_{ci}} v_{bqi}$. v_{bdi} and v_{bdi} are the dq components of v_b as exhibited in Fig. 1.

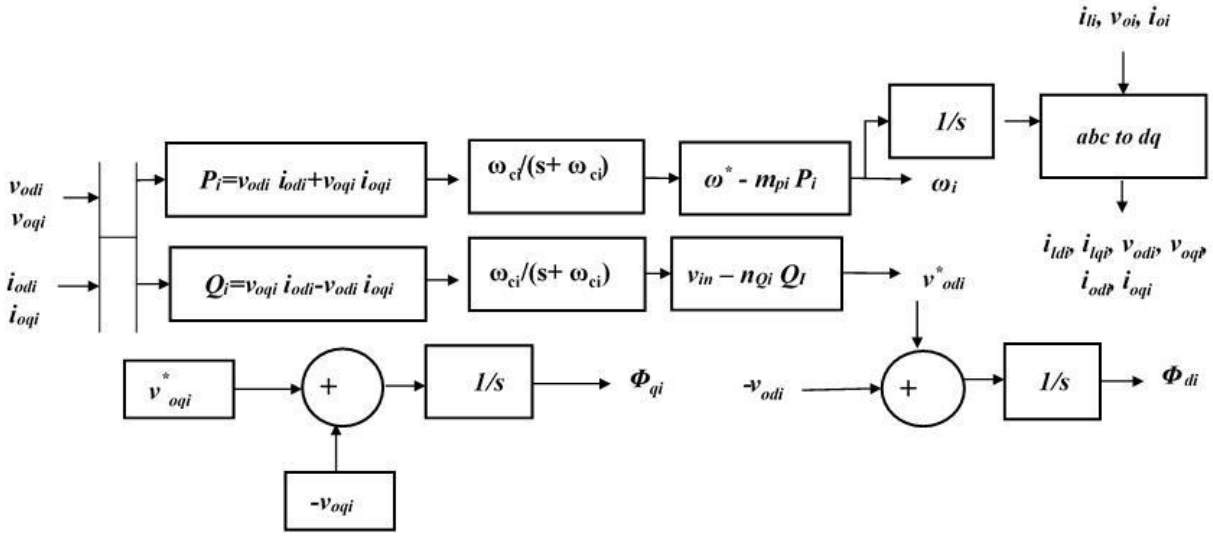

Fig. 2 The operating block diagram of the power loop in the robust primary controller.

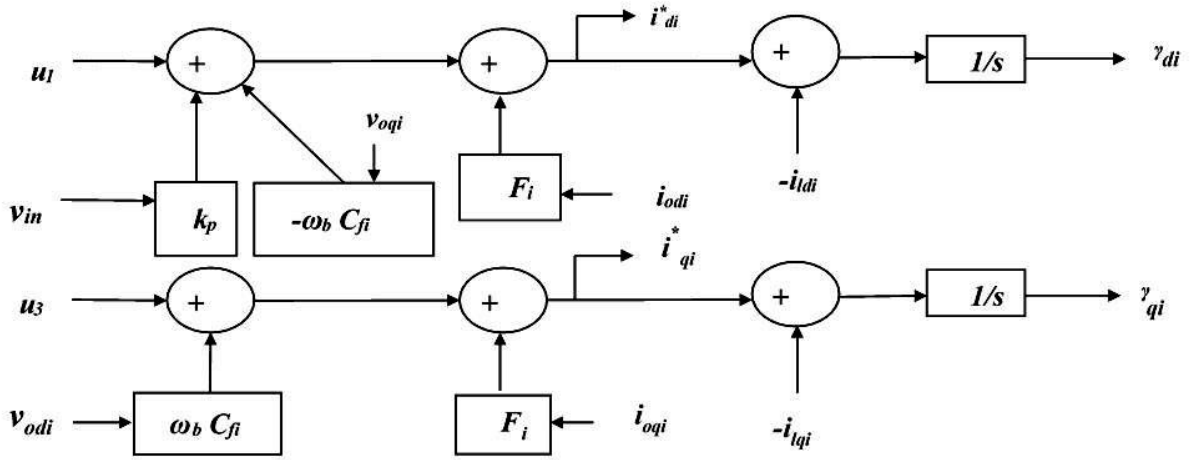

Fig. 3 The operating block diagram of the voltage loop in the robust primary controller.

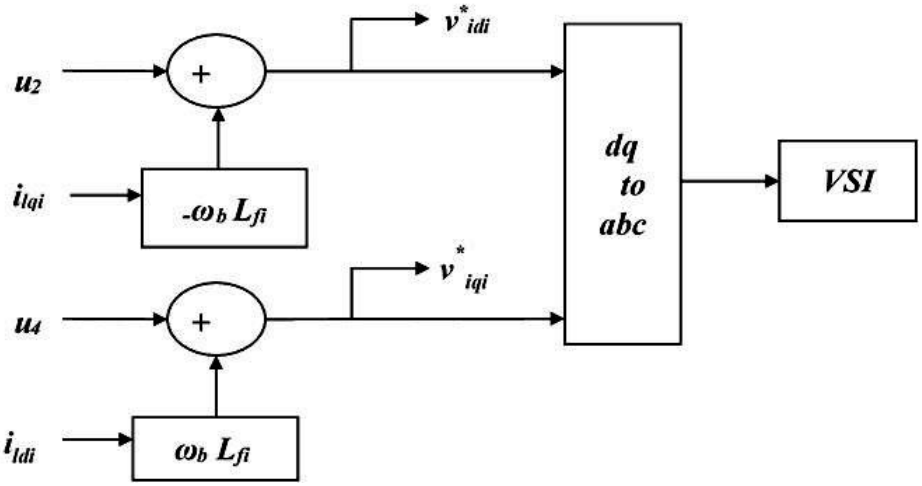

Fig. 4. The operating block diagram of the current loop in the robust primary controller.

2.2 The LPV Structure Preliminaries

The objective is to obtain an LPV representation of a standard state space equation, where the state vector is denoted by $x \in R^n$, the exogenous input by $w \in R^{n_w}$, the control input by $u \in R^{n_u}$, the control objective by $z_\infty \in R^{n_z}$, and the varying parameter by $\mu \in R^{\bar{\mu}}$, which is assumed to belong to a compact set as:

$$\begin{cases} \dot{x} = A(\mu)x + B_1(\mu)w + B_2(\mu)u \\ z_\infty = C(\mu)x \end{cases} \tag{21}$$

Assume that all matrices possess suitable dimensions and are confined within the polytope $\mathcal{P}$, which is defined as the convex hull of a finite set of matrices $\mathcal{H}_i$. The specified vertices are $(A_i, B_{1i}, B_{2i}, C_i, D_{1i}, D_{2i})$ for $i = 1,2,...,N$.

$$\begin{aligned} &\mathcal{H}(\mu) = \begin{pmatrix} A(\mu) & B_1(\mu) & B_2(\mu) \\ C(\mu) & D_1(\mu) & D_2(\mu) \end{pmatrix} \\ &\mathcal{H}_i = \begin{pmatrix} A_i & B_{1i} & B_{2i} \\ C_i & D_{1i} & D_{2i} \end{pmatrix}, i = 1,2,...,N \\ &\mathcal{H}(\mu) \in \mathcal{P} := Co\{\mathcal{H}_i, i = i = 1,2,...,N\} \\ &:= \left\{ \mathcal{H}(\mu) \,|\, \mathcal{H}(\mu) = \sum_{i=1}^{N} \alpha_i \mathcal{H}_i, \sum_{i=1}^{N} \alpha_i = 1, \alpha_i \geq 0 \right\} \end{aligned} \tag{22}$$

The H_∞ performance achievement is expressed by the synthesis of a control signal for (21) that provides the smallest attenuation level $\gamma > 0$ such that for any external input $w \in l_2$, it is verified that $Z_\infty \in l_2$, and:

$$\|Z_\infty\|_2 < \gamma \|w\|_2 \tag{23}$$

The subsequent lemma presents the requisite conditions for existence of a state-feedback gain matrix to achieve the stability of the closed-loop system, ensuring the attenuation level γ.

Lemma 1 [23-26]: The uncertain system (21) can be quadratically stabilized by the state feedback controller gain $K_{H_\infty LMI} = \Upsilon Q^{-1}$ with disturbance attenuation $\gamma > 0$, provided that there exist $Q = Q^T > 0$ and Υ of suitable dimensions that satisfy the following LMIs.

$$\begin{bmatrix} A_i Q + Q A_i^T + B_{2i}\Upsilon + \Upsilon^T B_{2i}{}^T & B_{1i} & QC_i^T + \Upsilon^T D_{2i}^T \\ B_{1i}^T & -I & D_{1i}^T \\ C_i Q + D_{2i}\Upsilon & D_{1i} & -\gamma^2 I \end{bmatrix} < 0 \quad (24)$$

$i = 1, 2, ..., N$

3 The Proposed LPV-Based Primary Control

In this section, the proposed LPV-based primary control is presented. The state vector of each DG is defined as:

$$x = [P \quad Q \quad \phi_d \quad \gamma_d \quad i_{ld} \quad v_{od} \quad i_{od} \quad \phi_q \quad \gamma_q \quad i_{lq} \quad v_{oq} \quad i_{oq}]^T \quad (25)$$

The state equations of the primary loops can be written as follows:

$$\dot{x}_1 = -\omega_c x_1 + \omega_{ci}(x_6 x_7 + x_{11} x_{12}) \quad (26)$$

$$\dot{x}_2 = -\omega_c x_2 + \omega_c(-x_6 x_{12} + x_{11} x_7) \quad (27)$$

$$\dot{x}_3 = -x_6 + v_{in} - n_Q x_2 \quad (28)$$

$$\dot{x}_4 = F x_7 - \omega_b C_f x_{11} - x_5 + k_p v_{in} + u_1 \quad (29)$$

$$\dot{x}_5 = -\frac{R_f}{L_f} x_5 - \frac{1}{L_f} x_6 + \frac{1}{L_f} u_2 \quad (30)$$

$$\dot{x}_6 = \frac{1}{C_f} x_5 - \frac{1}{C_f} x_7 + \omega^* x_{11} - m_P x_1 x_{11} \quad (31)$$

$$\dot{x}_7 = -\frac{R_c}{L_c} x_7 + \omega^* x_{12} - m_P x_1 x_{12} + \frac{1}{L_c} x_6 + d_1 \quad (32)$$

$$\dot{x}_8 = -x_{11} \quad (33)$$

$$\dot{x}_9 = F x_{12} + \omega_b C_f x_6 - x_{10} + u_3 \quad (34)$$

$$\dot{x}_{10} = -\frac{R_f}{L_f} x_{10} - \frac{1}{L_f} x_{11} + \frac{1}{L_f} u_4 \quad (35)$$

$$\dot{x}_{11} = -\omega^* x_6 + m_P x_1 x_6 + \frac{1}{C_f} x_{10} - \frac{1}{C_f} x_{12} \quad (36)$$

$$\dot{x}_{12} = \frac{-R_c}{L_c} x_{12} - \omega^* x_7 + m_P x_1 x_7 + \frac{1}{L_c} x_{11} + d_2 \quad (37)$$

The scheduling signal ($\rho \in R^9$) is defined as:

$$\rho := [x_7 \quad x_6 \quad x_{12} \quad x_{11} \quad C_f \quad R_f \quad L_f \quad L_c \quad R_c]^T \quad (38)$$

Therefore, by involving the scheduling signal via the defined varying parameters, equations (26)-(37) can be rewritten as:

$$\dot{x}_1 = -\omega_c x_1 + \mu_1 x_6 + \mu_2 x_7 + \mu_3 x_{11} + \mu_4 x_{12} \quad (39)$$

$$\dot{x}_2 = -\omega_c x_2 - \mu_3 x_6 + \mu_4 x_7 + \mu_1 x_{11} - \mu_2 x_{12} \quad (40)$$

$$\dot{x}_3 = -x_6 + v_{in} - n_Q x_2 \quad (41)$$

$$\dot{x}_4 = F x_7 + \mu_5 x_{11} - x_5 + u_1 \quad (42)$$

$$\dot{x}_5 = \mu_6 x_5 + \mu_7 x_6 + \frac{1}{L_f} u_2 \quad (43)$$

$$\dot{x}_6 = \mu_{11} x_1 + \mu_8 x_5 - \mu_8 x_7 + \omega^* x_{11} - \frac{m_P}{2} \beta x_{11} \quad (44)$$

$$\dot{x}_7 = \mu_{12} x_1 + \mu_9 x_6 + \mu_{10} x_7 + (\omega^* - \frac{m_p}{2}\beta) x_{12} + d_1 \quad (45)$$

$$\dot{x}_8 = -x_{11} \quad (46)$$

$$\dot{x}_9 = -\mu_5 x_6 - x_{10} + F x_{12} + u_3 \quad (47)$$

$$\dot{x}_{10} = \mu_6 x_{10} + \mu_7 x_{11} + \frac{1}{L_f} u_4 \quad (48)$$

$$\dot{x}_{11} = \mu_{13} x_1 + \frac{m_P}{2} \beta x_6 - \omega^* x_7 + \mu_8 x_{10} - \mu_8 x_{12} \quad (49)$$

$$\dot{x}_{12} = \mu_{14} x_1 + (-\omega^* + \frac{m_p}{2}\beta) x_7 + \mu_9 x_{11} + \mu_{10} x_{12} + d_2 \quad (50)$$

where β is power nominal value and,

$$\mu = [0.5\omega_c \rho_1 \quad 0.5\omega_c \rho_2 \quad 0.5\omega_{ci} \rho_3 \quad 0.5\omega_c \rho_4 \quad -\omega_b \rho_5 \quad -\frac{\rho_6}{\rho_7} \quad -\frac{1}{\rho_7} \quad \frac{1}{\rho_5} \quad \frac{1}{\rho_8} \quad -\frac{\rho_9}{\rho_5} \quad -0.5 m_P \rho_4 \quad -0.5 m_P \rho_3 \quad 0.5 m_P \rho_2 \quad 0.5 m_P \rho_1]^T \quad (51)$$

Therefore, the equations (39)-(50) can be formulated in a standard robust LPV-based problem compact form as below [27, 28]:

$$\dot{x} = A(\mu) x_i + B_1 w + B_2 u_\infty \quad z_\infty = Ce \quad (52)$$

where

$$w = \begin{bmatrix} v_{in} & d_1 & d_2 \end{bmatrix}^T \quad (53)$$

$$u_\infty = \begin{bmatrix} u_1 & \frac{1}{L_f} u_2 & u_3 & \frac{1}{L_f} u_4 \end{bmatrix}^T \quad (54)$$

$$e = [P \quad Q \quad \phi_d \quad \gamma_d \quad i_{ld} - i_{ld}^* \quad v_{od} - v_{od}^* \quad i_{od} \quad \phi_q \quad \gamma_q \quad i_{lq} - i_{lq}^* \quad v_{oq} \quad i_{oq}]^T \quad (55)$$

$$A(\mu)=\begin{bmatrix}
-\omega_c & 0 & 0 & 0 & 0 & \mu_1 & \mu_2 & 0 & 0 & 0 & \mu_3 & \mu_4 \\
0 & -\omega_c & 0 & 0 & 0 & -\mu_3 & \mu_4 & 0 & 0 & 0 & \mu_1 & -\mu_2 \\
0 & -n_Q & 0 & 0 & 0 & -1 & 0 & 0 & 0 & 0 & 0 & 0 \\
0 & 0 & 0 & 0 & -1 & 0 & F_i & 0 & 0 & 0 & \mu_5 & 0 \\
0 & 0 & 0 & 0 & \mu_6 & \mu_7 & 0 & 0 & 0 & 0 & 0 & 0 \\
\mu_{11} & 0 & 0 & 0 & \mu_8 & 0 & -\mu_8 & 0 & 0 & 0 & \omega^* - \frac{m_P}{2}\beta & 0 \\
\mu_{12} & 0 & 0 & 0 & 0 & \mu_9 & \mu_{10} & 0 & 0 & 0 & 0 & \omega^* - \frac{m_P}{2}\beta \\
0 & 0 & 0 & 0 & 0 & 0 & 0 & 0 & 0 & 0 & -1 & 0 \\
0 & 0 & 0 & 0 & 0 & -\mu_5 & 0 & 0 & 0 & -1 & 0 & F_i \\
0 & 0 & 0 & 0 & 0 & 0 & 0 & 0 & 0 & \mu_6 & \mu_7 & 0 \\
\mu_{13} & 0 & 0 & 0 & 0 & \mu_{13} & -\omega^* & 0 & 0 & \mu_8 & 0 & -\mu_8 \\
\mu_{14} & 0 & 0 & 0 & 0 & 0 & -\omega^* + \frac{m_P}{2}\beta & 0 & 0 & 0 & \mu_9 & \mu_{10}
\end{bmatrix} \tag{56}$$

$$B_1(\mu)=\begin{bmatrix}
0 & 0 & 1 & k_P & 0 & 0 & 0 & 0 & 0 & 0 & 0 & 0 \\
0 & 0 & 0 & 0 & 0 & 0 & 1 & 0 & 0 & 0 & 0 & 0 \\
0 & 0 & 0 & 0 & 0 & 0 & 0 & 0 & 0 & 0 & 0 & 1
\end{bmatrix}^T \tag{57}$$

$$B_2(\mu)=\begin{bmatrix}
0 & 0 & 0 & 1 & 0 & 0 & 0 & 0 & 0 & 0 & 0 & 0 \\
0 & 0 & 0 & 0 & 1 & 0 & 0 & 0 & 0 & 0 & 0 & 0 \\
0 & 0 & 0 & 0 & 0 & 0 & 0 & 0 & 1 & 0 & 0 & 0 \\
0 & 0 & 0 & 0 & 0 & 0 & 0 & 0 & 0 & 1 & 0 & 0
\end{bmatrix}^T \tag{58}$$

$$C=\begin{bmatrix}
0 & 0 & 1 & 0 & 0 & 0 & 0 & 0 & 0 & 0 & 0 & 0 \\
0 & 0 & 0 & 0 & 1 & 0 & 0 & 0 & 0 & 0 & 0 & 0 \\
0 & 0 & 0 & 0 & 0 & 1 & 0 & 0 & 0 & 0 & 0 & 0 \\
0 & 0 & 0 & 0 & 0 & 0 & 1 & 0 & 0 & 0 & 0 & 0 \\
0 & 0 & 0 & 0 & 0 & 0 & 0 & 0 & 0 & 1 & 0 & 0 \\
0 & 0 & 0 & 0 & 0 & 0 & 0 & 0 & 0 & 0 & 1 & 0
\end{bmatrix} \tag{59}$$

To formulate a polytopic model, it is necessary to consider three distinct values for every scheduling signal, namely the minimum, middle, and maximum values of its interval range. The production of $N=3^{\bar{\rho}}$ vertices is achieved by generating $\bar{\rho}=9$ scheduling signals, resulting in the notation of vertices by $J_i=(A_i,B_1,B_2,C)$. The system comprises 14 parameters denoted by $\bar{\mu}=14$, and a polytopic model necessitates $2^{\bar{\mu}}$ vertices. The substantial quantity of vertices necessitates a significant computational workload. Henceforth, we shall employ the PCA-based parameter set mapping technique to decrease the number of vertices. The DG dynamic model, however, will be restricted to the initial polytope.

$$\begin{cases}
\mathcal{P}_a=\left\{\mathcal{V}\middle|\mathcal{V}=\sum_{i=1}^{N}\alpha_i J_i,\ \sum_{i=1}^{N}\alpha_i=1,\alpha_i\geq 0\right\}\middle| \\
\mathcal{V}=(A(\mu),B_1,B_2,C)
\end{cases} \tag{60}$$

The polytope's vertices are denoted as $\mathcal{P}_a\ J_i$ concerning for $i=1,2,...,N$. The matrix denoted as $A(\mu)$ exhibits continuity for the parameter vector $\mu(t)\in R^{\bar{\mu}}$,and is contingent upon the scheduling signal $\rho(t)\in R^{\bar{\rho}}$, as dictated by $\mu(t)=\hbar(\rho(t))$. The continuous parameter mapping $\hbar\in R^{\bar{\rho}}\to R^{\bar{\mu}}$, as defined by (51), is also a contributing factor. The selection of the gridding points, denoted as N, is made with due consideration to the operating range of the system, nonlinearity effects, and the dimension of system parameters, ensuring that all dynamic behavior of the DG is comprehensively captured. The PCA technique is employed to perform parameter set mapping with the aim of identifying a reduced region within the parameter space. The polytopic model (60) is simplified by reducing its dimensionality to a lower-order area through the omission of minor directions in the mapped parameter space.

The methodology is described by the process in [29]. For the LPV model (52) and scheduling signal $\rho(t)$, the mapping $\eta(t)=r(\rho(t))\quad r:R^{\bar{\rho}}\to R^{\bar{\eta}}$ where $\bar{\eta}<\bar{\mu}$ should be found such that the reduced LPV model.

$$\begin{aligned}
\dot{x}&=\hat{A}(\eta)+B_1 w+B_2 u,\\
z_\infty&=Cx,
\end{aligned} \tag{61}$$

applied to approximate the model (52). The fundamental properties of PCA can be reviewed in [30].

The parameters of the polytopic LPV model (52) for $i=1,2,...,N$ are supposed to make a $\bar{\mu}\times N$ data matrix $\wp=[\mu^1,\mu^2,\ldots,\mu^N]$, where μ^i is the variable parameter vector evaluated at the i[th] vertex. Normalizing its rows with zero mean and standard unit deviation to construct the normalized data matrix $\wp^n=\prod(\wp)$. Subsequent, conduct the following singular value decomposition:

$$\wp^n=\begin{bmatrix}\hat{U} & U\end{bmatrix}\begin{bmatrix}\hat{\Sigma} & 0\\ 0 & \Sigma\end{bmatrix}\begin{bmatrix}\hat{\vartheta}^T\\ \vartheta^T\end{bmatrix} \tag{62}$$

Also, separating the $\bar{\eta}$ significant singular values coordinating to $\hat{U}$, $\hat{\Sigma}$, and $\hat{\vartheta}$, and neglecting the lower singular values leads to $\hat{\wp}^n=\hat{U}\hat{\Sigma}\hat{\vartheta}^T\approx\wp^n$, where $\hat{\wp}^n$ approximates the normalized given data $\wp^n$. The matrix $\hat{U}$ is used as a basis of the significant column space to realize the decreased mapping.

$$\eta(t)=\hat{U}^T\Pi(\hbar(\rho(t)))=\hat{U}^T\Pi(\mu(t)) \tag{63}$$

It means the approximate mapping of $\hat{A}(.)$ in (52) is related to (61) by

$$\hat{A}(\eta(t))=A(\hat{\mu}(t)) \tag{64}$$

where

$$\hat{\mu}(t)=\Pi^{-1}(\hat{U}\eta(t))=\Pi^{-1}(\hat{U}\hat{U}^T\Pi(\mu(t))) \tag{65}$$

attend that $\prod^{-1}$ reveals the row-wise rescaling. Hence, using $\hat{\wp}^n$ to restore the new vertices $(\hat{A}_i,B_1,B_2,C)$, the polytopic LPV model (60) is decreased to

$$\begin{cases}\hat{\mathcal{H}}(\mu):=(\hat{A}(\hat{\mu}),B_1,B_2,C)\\ \hat{\mathcal{H}}_i:=(\hat{A}_i,B_{1i},B_{2i},C),i=1,2,...,\hat{N}\\ \hat{\mathcal{P}}:=\{\hat{\mathcal{H}}(\mu)\,|\,\hat{\mathcal{H}}(\mu)=\sum_{i=1}^{\hat{N}}\alpha_i\,\hat{\mathcal{H}}_i,\sum_{i=1}^{\hat{N}}\alpha_i=1,\alpha_i\geq 0\}\end{cases} \tag{66}$$

The variable $\hat{N}=2^{\bar{\eta}}$ represents the number of vertices, while $(\hat{A}_i,B_1,B_2,C)$ denotes the model of the i[th] new vertex. The fraction of the total variation, V_η, can be presented as a standard for measuring the quality of the approximated polytopic model (66) relative to the actual polytopic model (60) by the singular values in (62).

$$V_\eta=\sum_{i=1}^{\bar{\eta}}\sigma_i^2\Big/\sum_{i=1}^{\bar{\mu}}\sigma_i^2 \tag{67}$$

The appropriate selection of $\bar{\eta}$ is demonstrated in Figure 5 through the utilization of relation (67) across various $\bar{\eta}$. Subsequently, the appropriate $\bar{\eta}=6$ is ascertained based on the preferred acceptable percentage of error in the recorded data. Approximately 85% of the information is constituted by data, and the P-LPV model (66) in its simplified form will solely encompass $\hat{N}=2^6=64$ vertices.

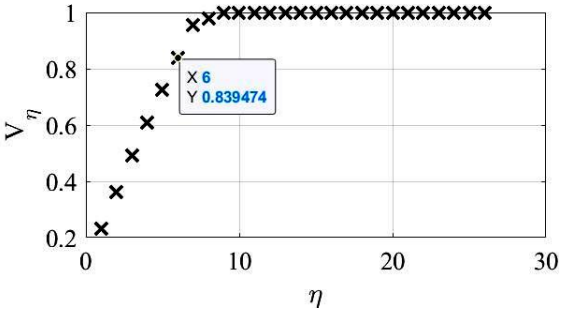

Fig. 5 Fraction of total variation V_η versus $\bar{\eta}$.

The proposed controller $K_{H_\infty LMI}$ is obtained by solving LMI (24). The standard form of the proposed H_∞ synthesis LPV-based problem for the IMG is shown in Fig. 6.

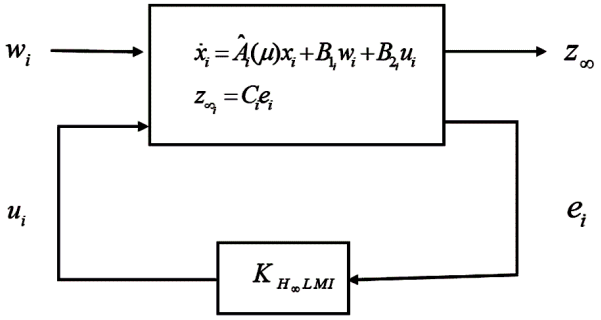

Fig. 6 The standard form of the proposed H_∞ synthesis LPV-based problem for the IMG.

4 Simulation Results

To demonstrate the authenticity of the proposed robust primary control, a simulation is conducted in MATLAB/Sim-Power System environment. The simulation involves an AC test-IMG 380 V, 50 Hz system comprising four DG units and two loads, as illustrated in Figure 7.

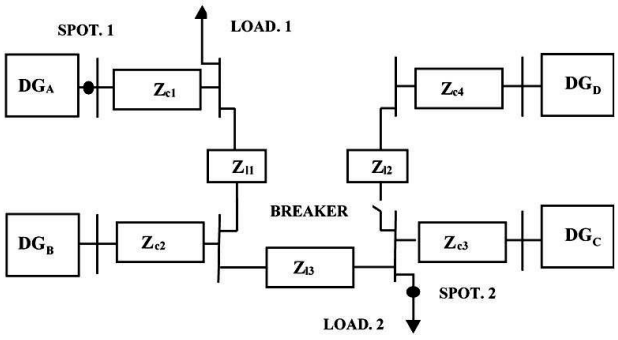

Fig. 7 The schematic of the Test-IMG.

Table 1 presents the test system parameters. In order to assess the efficacy of the method in terms of robustness and efficiency, various scenarios, such as load bar

alteration, faults, and reconfiguration, are implemented on the test-IMG. The efficacy of the proposed method is assessed by comparing it with the conventional primary control method described in the reference [20].

Table 1 The test system parameters.

Description	DGA & DGB (45 kVA)	*DGC& DGD* (34 kVA)
($R_c(\Omega)$, L_c(mH))	(0.03,0.35)	(0.03,35)
$R_f(\Omega)$	0.1	0.1
L_f(mH)	1.35	1.35
$C_f(\mu F)$	50	50
m_P	0.000094	0.000125
n_Q	0.0013	0.0015
	Lines	
Z_{l1}: ($R_{l1}(\Omega)$, $L_{l1}(\mu H)$)	(0.23,318)	
Z_{l2}: ($R_{l2}(\Omega)$, $L_{l2}(\mu H)$)	(0.35,1847)	
Z_{l3}: ($R_{l3}(\Omega)$, $L_{l3}(\mu H)$)	(0.23,318)	
	Loads	
P_{L1} (kW), Q_{L1} (kVAR)	(12,12)	
P_{L2} (kW), Q_{L2} (kVAR)	(15.3,7.6)	

Description	***Gain factor [20]***	***DG A&B [20]***	***DG C&D [20]***
Power control Gain [20]	mPi	0.000094	0.000125
	nQi	0.0013	0.00150
Voltage control Gain [20]	KPVi	0.1	0.05
	KIVi	420	390
Current control Gain [20]	KPCi	15	10.5
	KICi	20000	16000
Description	*Ranges*		
Scheduling parameters of the proposed method	$\rho_1 = 28 \pm 20\%, \rho_2 = 537 \pm 10\%,$ $\rho_3 = -48 \pm 35\%, \rho_4 = 0 \pm 0.15,$ $\rho_5 = 5\times10^{-5} \pm 10\%, \rho_6 = 0.1 \pm 10\%,$ $\rho_7 = 1.35\times10^{-3} \pm 10\%, \rho_8 = 3.5\times10^{-2} \pm 10\%,$ $\rho_9 = 0.03 \pm 10\%$		

4.1 Appraisement of the Proposed Robust Primary Controller Under Periodic Load Bar Altering Scenarios

This section conducts load bar alteration scenarios to validate the proposed methods. The test-IMG was subjected to the proposed robust primary controller at t=0 seconds. Table 2 enumerates the periodic load-bar modification scenarios. Figures 8 to 11 depict the variations in frequency, active power, RMS voltage (pu), and reactive power, respectively. The stability of both frequency and voltage variation indicates the fulfillment of the power-sharing arrangement.

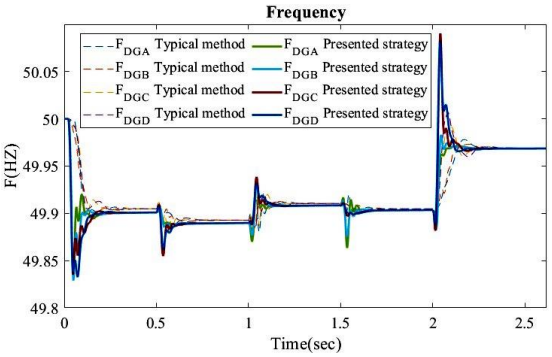

Fig. 8 The frequency variations of Test-IMG in the case of loads-changing scenarios.

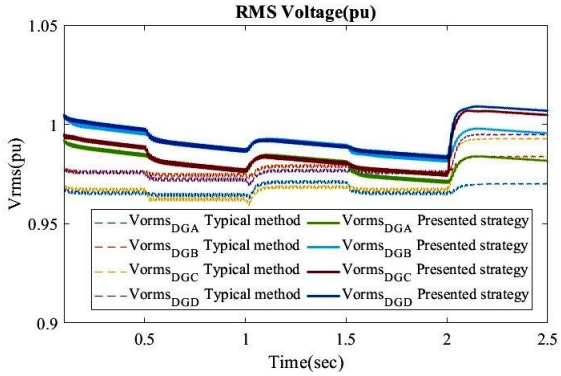

Fig. 9 The RMS voltage (pu) variations of Test-IMG in the case of loads-changing scenarios.

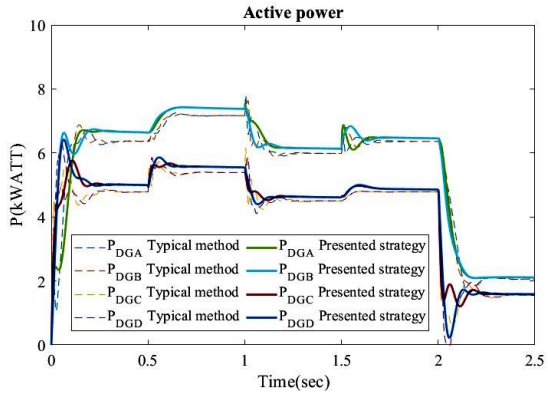

Fig. 10 The active power variations of Test-IMG in the case of loads-changing scenarios.

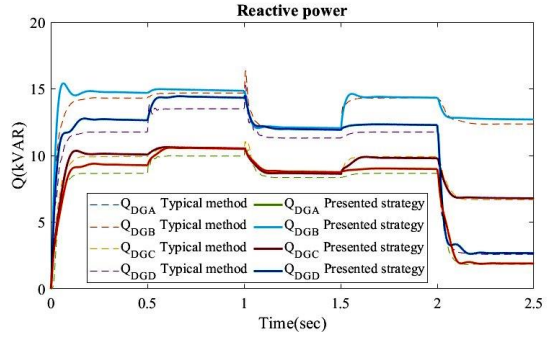

Fig. 11 The reactive power variations of Test-IMG in the case of loads-changing scenarios.

Table 2 The load bar change scenarios.

Description of scenarios	Load. 1 (P_{L1}, Q_{L1})	Load. 2 (P_{L2}, Q_{L2})
0<t<0.5	(P_{L1}, Q_{L1})	(P_{L2}, Q_{L2})
0.5<t<1	(P_{L1}, Q_{L1})	1.2(P_{L2}, Q_{L2})
1<t<1.5	0.8(R_{L1}, L_{L1})	(P_{L2}, Q_{L2})
1.5<t<2	(P_{L1}, Q_{L1})	(P_{L2}, Q_{L2})
2<t	(P_{L1}, Q_{L1})	Disconnected

4.2 Appraisement of the Proposed Robust Primary Controller Under the Fault Scenarios

The presented method's validity performance is verified through the execution of single and three-phase-to-ground faults in this scenario. The initial occurrence involves a three-phase-to-ground fault at location spot two at time t=0.4 sec, followed by a subsequent single-phase-to-ground fault at location spot one at time t=1.5 sec. The temporal extent of faults is 0.01 and 0.05 seconds, respectively. Figures 12 to 15 display the variations in frequency, active power, RMS voltage (pu), and reactive power of DG_A. The findings demonstrate that the proposed approach exhibits prompt restoration to its steady state upon rectifying the transient time. Conversely, the conventional approach experiences instability during the three-phase-to-ground fault. The findings indicate that the suggested approach exhibits superior and robust performance compared to the standard response.

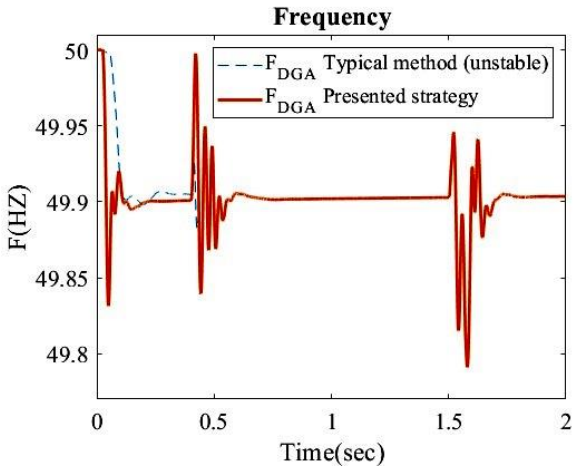

Fig. 12 The frequency variations of Test-IMG in the case of a fault scenario.

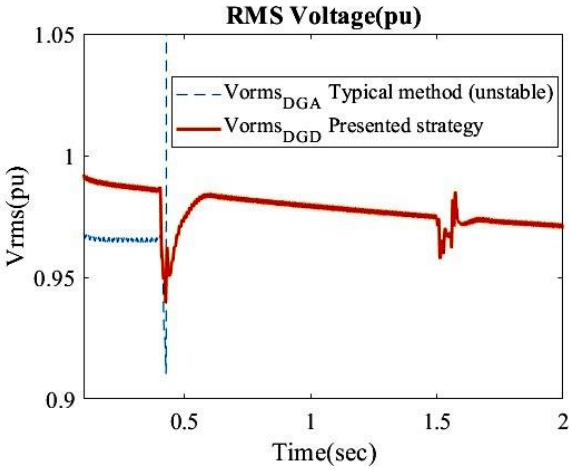

Fig. 13 The RMS voltage (pu) variations of the DG_A between the conventional method and the proposed method in the case of a fault scenario.

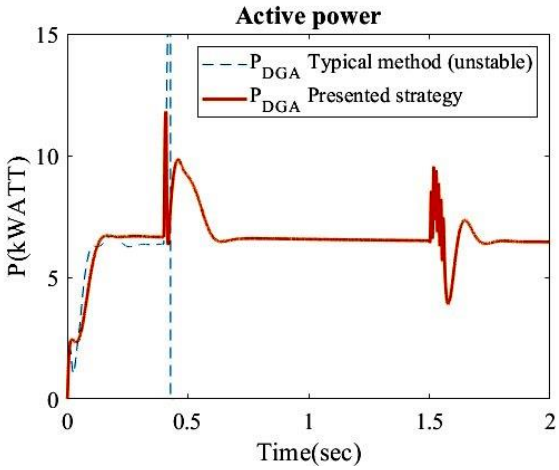

Fig. 14 The active power variations of the DG_A between the conventional method and the proposed method in the case of a fault scenario.

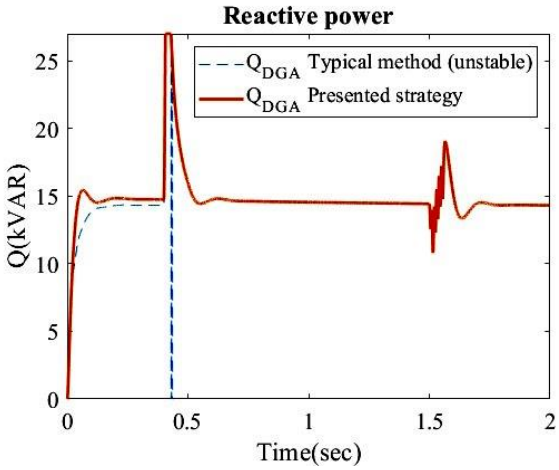

Fig. 15 The reactive power variations of the DG_A between the conventional method and the proposed method in the case of a fault scenario.

4.3 Appraisement of the Proposed Robust Primary Controller for the Reconfiguration Scheme Scenario

This section aims to reconfigure the structure of test-IMG to verify the robustness of the strategy that has been presented. The scenarios above have been subjected to testing. The controller initiates operation at t=0. At t=0.5, the three-phase breaker is opened, resulting in the disconnection of DG_D from the MG. At t=1.5, breaker-A is closed, allowing for the reconnection of DG_D. Figures 16 to 19 illustrate the variations in frequency, active power, RMS voltage (pu), and reactive power of DG_A. The findings indicate that the suggested controller effectively averts system instability, whereas the conventional controller's employment leads to the test-IMG's instability. Thus, the proposed method exhibits a higher level of robustness than the traditional method.

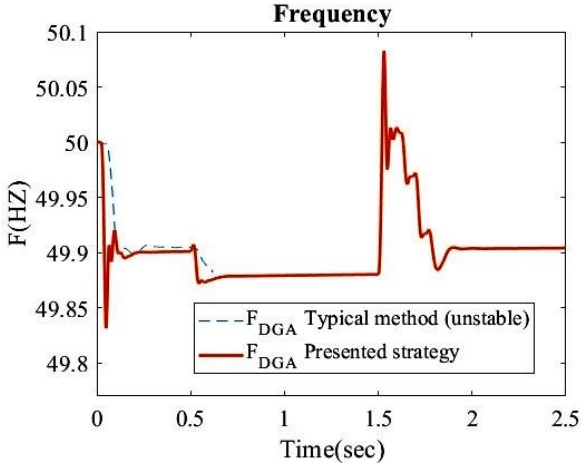

Fig. 16 The frequency variations of Test-IMG in the case of structure reconfiguration scenario.

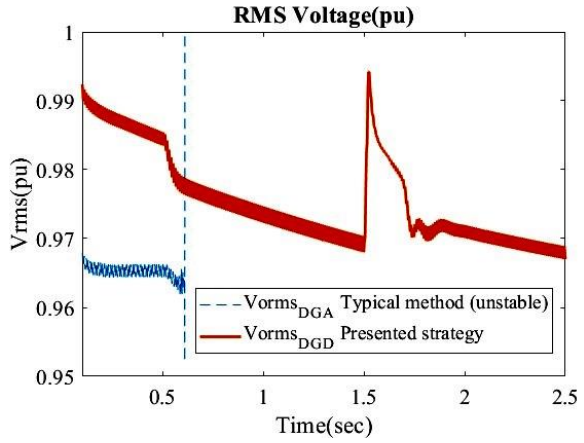

Fig. 17 The RMS voltage (pu) variations of the DG_A between the conventional method and the proposed method in the case of structure reconfiguration scenario

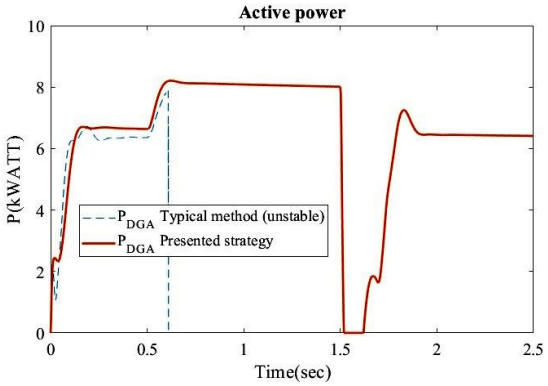

Fig. 18 The active power variations of the DG_A between the conventional and proposed methods in the structure reconfiguration scenario.

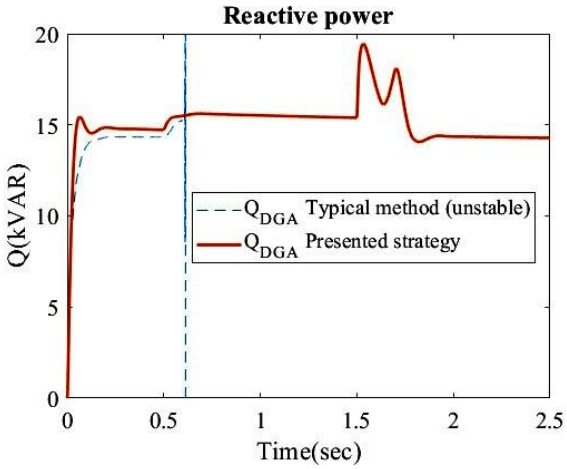

Fig. 19 The reactive power variations of the DG_A between the conventional method and proposed method in the case of structure reconfiguration scenario.

5 Conclusion

This article presents a novel primary controller for the AC IMG based on LPV modeling and a robust H∞- LMI approach. The controller aims to effectively regulate the frequency and voltage of the IMG under various scenarios, such as load changes, faults, and reconfigurations. Moreover, the controller takes into account the nonlinearity and uncertainty of the system parameters, which are often neglected in previous works. The system dynamics are represented as a polytopic LPV model in the innovative primary control structure. The state-feedback control is computed by solving the corresponding LMIs based on H∞ performance and stability criteria. The proposed robust primary control is applied to a test IMG in the SIM-POWER environment of MATLAB and evaluated under different scenarios. The simulation results demonstrate the validity, effectiveness, and superiority of the proposed method in stabilizing the frequency and voltage of the AC IMG. As a future work, the same method can be extended to control the DC MG as well.

References

[1] S. Choudhury, "Review of Energy Storage System Technologies Integration to Microgrid: Types, control strategies, issues, and future prospects," *Journal of Energy Storage*, vol. 48, p. 103966, 2022.

[2] B. Fani, G. Shahgholian, H. H. Alhelou, and P. Siano, "Inverter-Based Islanded Microgrid: A Review on Technologies and Control," *e-Prime-Advances in Electrical Engineering, Electronics and Energy*, p. 100068, 2022.

[3] N. P. Srinivas and S. Modi, "A Comprehensive Review of Microgrids, Control Strategies, and Microgrid Protection Schemes," *ECS Transactions*, vol. 107, no. 1, p. 13345, 2022.

[4] K. A. Tahir, M. Zamorano, and J. O. García, "Scientific mapping of optimization applied to microgrids integrated with renewable energy systems," *International Journal of Electrical Power & Energy Systems*, vol. 145, p. 108698, 2023.

[5] G. S. Thirunavukkarasu, M. Seyedmahmoudian, E. Jamei, B. Horan, S. Mekhilef, and A. Stojcevski, "Role of optimization techniques in microgrid energy management systems—a review," *Energy Strategy Reviews*, vol. 43, p. 100899, 2022.

[6] A. K. Hamid, N. T. Mbungu, A. Elnady, R. C. Bansal, A. A. Ismail, and M. A. AlShabi, "A systematic review of grid-connected photovoltaic and photovoltaic/thermal systems: Benefits, challenges and mitigation," *Energy & Environment*, p. 0958305X221117617, 2022.

[7] H. Sridevi, S. Jagwani, and H. Ravikumar, "Recent Intelligent Optimisation Algorithms for Islanded Microgrids: A Review," *Emerging Research in Computing, Information, Communication and Applications*, pp. 743-753, 2022.

[8] A. Zakipour, K. Aminzare, and M. Salimi, "Sliding Mode Controller Design for Stabilization of the Three-Phase Grid-Connected Inverters in the Presence of Unbalanced Local Loads," (in eng), *Iranian Journal of Electrical and Electronic Engineering*, Research Paper vol. 18, no. 3, pp. 2125-2125, 2022, doi: 10.22068/ijeee.18.3.2125.

[9] S. Ishaq, I. Khan, S. Rahman, T. Hussain, A. Iqbal, and R. M. Elavarasan, "A review on recent developments in control and optimization of microgrids," *Energy Reports*, vol. 8, pp. 4085-4103, 2022.

[10] M. Raeispour, H. Atrianfar, H. R. Baghaee, and G. B. Gharehpetian, "Resilient H∞ consensus-based control of autonomous AC microgrids with uncertain time-delayed communications," *IEEE Transactions on Smart Grid*, vol. 11, no. 5, pp. 3871-3884, 2020.

[11] M. Raeispour, H. Atrianfar, H. R. Baghaee, and G. B. Gharehpetian, "Robust Distributed Disturbance-Resilient H∞-Based Control of Off-Grid Microgrids With Uncertain Communications," *IEEE Systems Journal*, vol. 15, no. 2, pp. 2895-2905, 2021, doi: 10.1109/JSYST.2020.3001243.

[12] A. Afshari, M. Karrari, H. R. Baghaee, G. B. Gharehpetian, and J. M. Guerrero, "Robust Cooperative Control of Isolated AC Microgrids Subject to Unreliable Communications: A Low-Gain Feedback Approach," *IEEE Systems Journal*, vol. 16, no. 1, pp. 55-66, 2021.

[13] M. B. A. Jabali and M. H. Kazemi, "A new LPV modeling approach using PCA-based parameter set mapping to design a PSS," *Journal of Advanced Research*, vol. 8, no. 1, pp. 23-32, 2017.

[14] M. B. A. Jabali and M. H. Kazemi, "Uncertain polytopic LPV modeling of robot manipulators and trajectory tracking," *International Journal of Control, Automation and Systems*, vol. 15, no. 2, pp. 883-891, 2017.

[15] S. Azizi, M. H. Asemani, N. Vafamand, S. Mobayen, and A. Fekih, "Adaptive Neural Network Linear Parameter-Varying Control of Shipboard Direct Current Microgrids," *IEEE Access*, vol. 10, pp. 75825-75834, 2022.

[16] N. Mohammed, W. Zhou, and B. Bahrani, "Comparison of PLL-Based and PLL-Less Control Strategies for Grid-Following Inverters Considering Time and Frequency Domain Analysis," *IEEE Access*, vol. 10, pp. 80518-80538, 2022.

[17] M. Dehghani *et al.*, "Control of LPV Modeled AC-Microgrid Based on Mixed H 2/H∞ Time-Varying Linear State Feedback and Robust Predictive Algorithm," *IEEE Access*, vol. 10, pp. 3738-3755, 2021.

[18] S. Asadi, N. Vafamand, M. Moallem, and T. Dragičević, "Fault reconstruction of islanded nonlinear DC microgrids: An LPV-based sliding mode observer approach," *IEEE Journal of Emerging and Selected Topics in Power Electronics*, vol. 9, no. 4, pp. 4606-4614, 2020.

[19] A. Aff, M. Simab, M. Nafar, and A. Mirzaee, "Robust linear parameter varying frequency control for islanded hybrid AC/DC microgrids," *Electric Power Systems Research*, vol. 214, p. 108898, 2023/01/01/ 2023, doi: 10.1016/j.epsr.2022.108898.

[20] A. Bidram, F. L. Lewis, and A. Davoudi, "Distributed control systems for small-scale power networks: Using multiagent cooperative control theory," *IEEE Control Systems Magazine*, vol. 34, no. 6, pp. 56-77, 2014.

[21] J. Hu and P. Bhowmick, "A consensus-based robust secondary voltage and frequency control scheme for islanded microgrids," *International Journal of Electrical Power & Energy Systems*, vol. 116, p. 105575, 2020.

[22] M. Keshavarz, A. Doroudi, M. H. Kazemi, and N. M. Dehkordi, "A novel adaptive distributed secondary voltage controller with high convergence rate for islanded microgrids," *IEEE Systems Journal*, vol. 15, no. 3, pp. 4157-4167, 2020.

[23] P. P. Khargonekar and M. A. Rotea, "Mixed H_2/H_∞ infinity/control: a convex optimization approach," *IEEE Transactions on Automatic Control*, vol. 36, no. 7, pp. 824-837, 1991.
[24] W. J. Rugh and J. S. Shamma, "Research on gain scheduling," *Automatica*, vol. 36, no. 10, pp. 1401-1425, 2000.
[25] J. S. Shamma, "An Overview of LPV Systems," in *Control of Linear Parameter Varying Systems with Applications*, J. Mohammadpour and C. W. Scherer Eds. Boston, MA: Springer US, 2012, pp. 3-26.
[26] H. Wu and Y. Fei, "Mixed H2/H∞ guaranteed-cost control for uncertain linear systems," *IFAC Proceedings Volumes*, vol. 32, no. 2, pp. 3508-3513, 1999.
[27] J. Mohammadpour and C. W. Scherer, *Control of linear parameter varying systems with applications*. Springer Science & Business Media, 2012.
[28] J. S. Shamma, "An overview of LPV systems," *Control of linear parameter varying systems with applications*, pp. 3-26, 2012.
[29] A. Kwiatkowski and H. Werner, "PCA-based parameter set mappings for LPV models with fewer parameters and less overbounding," *IEEE Transactions on Control Systems Technology*, vol. 16, no. 4, pp. 781-788, 2008.
[30] I. T. Jolliffe, *Principal component analysis for special types of data*. Springer, 2002.
[31] A. Fazli and M. H. Kazemi, "Manipulator Dynamic Nonlinearity Approximation Based on Polytopic LPV Modeling for Robot Tracking Control Problem," *Iranian Journal of Science and Technology, Transactions of Electrical Engineering*, vol. 46, no. 2, pp. 537-547, 2022/06/01 2022, doi: 10.1007/s40998-021-00477-y.

AUTHOR INFORMATION

Fatemeh Zare-Mirkabad received her bachelor's and master's degrees in biomedical-clinical engineering and electrical-control engineering from Shahed University, Tehran, Iran, in 2013 and 2016, respectively. She is researching as a Ph.D. candidate in electrical-power engineering at Shahed University and working as an expert electrical engineer at HISTACO company. She taught as a visiting lecturer at PNU University and Shahed University (2018-2020) and worked as an expert electrical engineer at Moshanir Power Engineering Consultants Company (Moshanirco) in Iran (2021-2023). Her research background is as follows: Microgrid Control, Electrical Railway, Robust Control, Tunnel lighting design, CCTV system design, Radio system design.

Mohammad Hossein Kazemi received his B.Sc. degree in electrical engineering from the Khajeh Nasir University, Tehran, Iran, and M.Sc. and Ph.D. degrees in electrical-control engineering from Sharif University and Amirkabir University, Tehran, Iran, in 1995 and 2011, respectively. He works as an Associate Professor in the Department of Electrical Engineering at Shahed University, Tehran, Iran. His research interest is as follows: Robotics, Power Systems, Robust and Adaptive control, and Microgrid Control.

Aref Doroudi received his B.Sc., M.Sc., and Ph.D. in electrical-power engineering from Amirkabir University, Tabriz University, and Amirkabir University, Iran, in 1992, 1994, and 2000, respectively. He works as an Associate Professor in the Department of Electrical Engineering at Shahed University, Tehran, Iran. His research interest is as follows: Power Quality, Electrical Machine Design, Power Systems Dynamic, Resilience, and Microgrid Control.